Proceedings of Fifth Annual Inverse Problems in Engineering Seminar,
June 11 - 12, 1992, Michigan State University, East Lansing, MI,
Editor: James V. Beck

INVERSE DESIGN AND OPTIMIZATION IN AEROTHERMODYNAMICS

George S. Dulikravich
Department of Aerospace Engineering
The Pennsylvania State University, University Park, PA 16802, USA

Abstract

Aerodynamic shape design is performed using inverse methods and optimization. Inverse methods are much more common, while optimization methods involving sensitivity analysis and adjoint operator approach are only becoming popular. Research in this area is expected to concentrate on the use of Navier-Stokes equations and applications to three-dimensional configurations. Interdisciplinary constrained optimization is expected to play a more prominent role in the immediate future, while adjoint operator/control theory are the most promising concepts for interdisciplinary aerodynamic shape design which involves a large number of variables.

Introduction

In the case of an aerodynamic shape design we are asked to predict the geometry of an object, which must be compatible with the desired features of the flow field. Thus, aerodynamic shape design involves the ability to determine the geometry of an aerodynamic object that will satisfy the governing equations for the flow field and the desired boundary conditions. For example, it is possible to determine the coordinates of an airfoil if a surface pressure distribution is specified. The resulting designs can be subject to certain specified constraints. Examples which include such constraints may entail finding aerodynamic configurations that are compatible with entirely shock-free transonic flow fields or obtaining shapes of objects that produce flow fields with minimum entropy generation, minimum noise generation, desired surface heat flux distribution, etc.

Depending on the prescribed features of the flow field, design (inverse) methodologies can be grouped into two general categories: surface flow design and flow field design. Surface flow design involves specifying certain flow parameters (pressure, Mach number, etc.) on the surface of the flying object, then finding the shape that will generate these surface conditions without regard for the rest of the flow field. Flow field design approach, on the other hand, enforces certain global flow field features (shock-free flow, minimal entropy generation, etc.) at every point of the flow field by determining the shape that will satisfy these constraints locally. A large number of methods for performing surface flow design have been developed, while only a few methods for flow field design are known to exist.

Although numerous methods[1-6] for performing inverse design and optimization of aerodynamic configurations have been devised, these methods are not routinely used by the engineering community. Since there are no comprehensive textbooks covering this field (except for a few publications in the form of survey articles), these methods have not been taught in engineering programs. Consequently, present and future engineers are inadequately trained in this rapidly growing field. In other words, future aerodynamicists are not taught how to achieve the mathematically optimal aerodynamic configurations most economically via inverse design and optimization. Instead, cut-and-try design based on repetitive analysis and intuition is still widely practiced in the aerospace industry. Needless to say, this classical inefficient approach cannot survive the rigors of the competitive global world market. This fact has been recognized by a few leading companies where these methods are being developed and implemented by a few highly specialized individuals. These efforts, although resulting in actual hardware, have been mostly covered by a veil of undue secrecy. This concise survey article is an attempt to classify and briefly evaluate the most prominent aerodynamic design methods available in the open literature.

One of the reasons for the slow acceptance of inverse design and optimization methodologies in the field of aerodynamics has been the notion that these methods are hard to

comprehend and difficult to mathematically formulate. The fact is that most of the design methods are as complex analytically and numerically as their direct (analysis) counterparts. A typical inverse design computer code needs a single run to generate a new shape that duplicates the desired surface flow parameters. An advanced constrained optimization code might require computer time that is equivalent to a few dozen analysis runs in order to arrive at a mathematically optimal configuration rather than just an improved shape that the cut-and-try approach would be able to provide. The arbitrary distribution of the surface flow parameters or an arbitrary field distribution of the flow parameters could result in shapes that are not physically meaningful and cannot be manufactured. For example, the lower surface and the upper surface of an airfoil could either cross over ("fish tail shapes") or never meet (open trailing edge shapes) although these solutions are mathematically acceptable. Obviously, the problem rests in choosing an appropriate surface distribution of the flow parameters that satisfies certain global flow field constraints and certain constraints on the geometry since the final aerodynamic design is often incompatible with heat transfer, structural dynamics, acoustics, or manufacturing requirements.

Most of the aerodynamic inverse design methods have been available for quite some time. Mathematical models used in aerodynamic shape design are based on partial differential equations, integral equations, and algebraic equations. Detailed reviews have been presented at specialists meetings[1-5] in the form of survey articles[6].

The main objection raised by designers when discussing inverse design methodologies is that these methods create strictly point-designs rather than range-designs. In other words, an aerodynamic shape designed by using a surface flow design method will have the desired characteristics only at the design conditions.

Although numerous methods for performing inverse design and optimization of aerodynamic configurations have been devised, these methods are not routinely used by the engineering community. Moreover, since there are no comprehensive publications in the form of survey articles and textbooks, these methods have not been taught in the engineering programs. Consequently, present and future engineers are inadequately trained in this rapidly growing field. In other words, the future aerodynamicists are not taught how to achieve the mathematically optimal aerodynamic configurations most economically via inverse design and constrained optimization. Instead, cut-and-try design based on repetitive analysis and intuition is still widely practiced in our aerospace industry. Needless to say, this classical inefficient approach cannot survive the rigors of the competitive global world market. This fact has been recognized by a few leading companies (e.g. Boeing, Lockheed, Grumman, Pratt & Whitney, General Electric) where these methods are being developed and implemented by a few highly specialized individuals. These efforts, although resulting in actual hardware, have been mostly covered by a veil of undue secrecy. NASA, except for a few isolated efforts carried out by individual researchers, has not shown any inclination in the past to support organized research on the inverse methods and optimization in the field of aerodynamics, although it has actively and successfully supported development of similar methodologies in the field of structural design.

It should be pointed out that one of the possible reasons for the slow acceptance of the inverse design and optimization methodologies in the field of aerodynamics in the past has been the notion that these methods are usually harder to comprehend and to mathematically formulate. The fact is that most of these methods are equally complex analytically and numerically as their direct (analysis) counterparts. While a typical inverse design computer code needs a single run to generate a new shape that duplicates the desired surface flow parameters, an advanced constrained optimization code might require computer time that is equivalent to a dozen analysis runs in order to arrive at a mathematically optimal configuration rather than just an improved shape that the cut-and-try approach would be able to provide.

In other countries where resources are not as plentiful, the approach to and the acceptance of the inverse design and optimization in aerodynamics has been more organized. Specifically, there are several research institutes in the USSR and an institute in the P.R. China that are devoted to developing these methodologies. In France, ONERA, as a French equivalent of NASA, actively develops these methods in close collaboration with their industry (e.g., SNECMA, Dassault)

where the methods are immediately implemented in the design process. In The Netherlands, NLR has an entire group of researchers developing interdisciplinary optimization techniques and interacting with their aerospace industry. In Italy, University of Torino and Fiat Company have a very active and productive program in the area of inverse design of turbomachinery configurations. In Germany, DLR and MBB have been successfully interacting on the development of inverse design methods for Airbus shock-free wing. MBB is presently perfecting a new methodology for optimization of a complete three-dimensional airplane configuration.

In the author's opinion, the new methods in aerodynamic shape design and optimization will be perfected and become more widely used when: a) we overcome a psychological barrier of learning a conceptually new approach to design, and b) the foreign competition forces us to do so.

Most of the methods that will be mentioned in this article have been available for quite some time. It was the author's deliberate decision to quote only the methods that have either found their acceptance in industry or that could be further perfected. Publications detailing methods of inverse design are more numerous than the articles describing the optimization-based methods. Thus, the author would like to apologize for not being able to quote all the publications available and for focusing more on the inverse design methods.

References

1. *Proceedings of the 1st International Conference on Inverse Design Concepts and Optimiz. in Eng. Sci. (ICIDES-I),* ed. G.S. Dulikravich, Dept. of Aero. Eng. and Eng. Mech., Univ. of Texas, Austin, TX, Oct. 17-18, 1984.
2. *Proceedings of the 2nd International Conference on Inverse Design Concepts and Optimiz. in Eng. Sci. (ICIDES-II),* ed. G.S. Dulikravich, Dept. of Aero. Eng., Penn State Univ., University Park, PA, Oct. 26-28, 1987.
3. *Proceedings of the AGARD Specialist's Meeting on Computational Methods for Aerodynamic Design (Inverse) and Optimization,* AGARD CP-463, ed. J. W. Slooff, Loen, Norway, May 24-25, 1989.
4. *Proceedings of a Special Course on Inverse Methods for Airfoil Design for Aeronautical and Turbomachinery Applications*, ed. R. Van Dem Braembusche, AGARD Report No. 780, Rhode-St.-Genese, Belgium, May 14-18, 1990.
5. *Proceedings of the 3rd International Conference on Inverse Design Concepts and Optimiz. in Eng. Sci. (ICIDES-III),* ed. G.S. Dulikravich, Washington, D.C., October 23-25, 1991.
6. Dulikravich, G.S., "Aerodynamic Shape Design and Optimization: Status and Trends", AIAA paper 91-0476, Aerospace Sciences Meeting, Reno, NV, Jan. 7-10, 1991; also to appear in *AIAA Journal of Aircraft,* Sept./Oct. 1992.

WHY:

- Foreign Competition: PRC, USSR, Japan, FRG, France, Italy, etc.

- ICIDES-I, ICIDES-II, AGARD:
  more organized approach in the West

- Economic Efficiency

WIND TUNNEL TEST PROGRAM
TRENDS

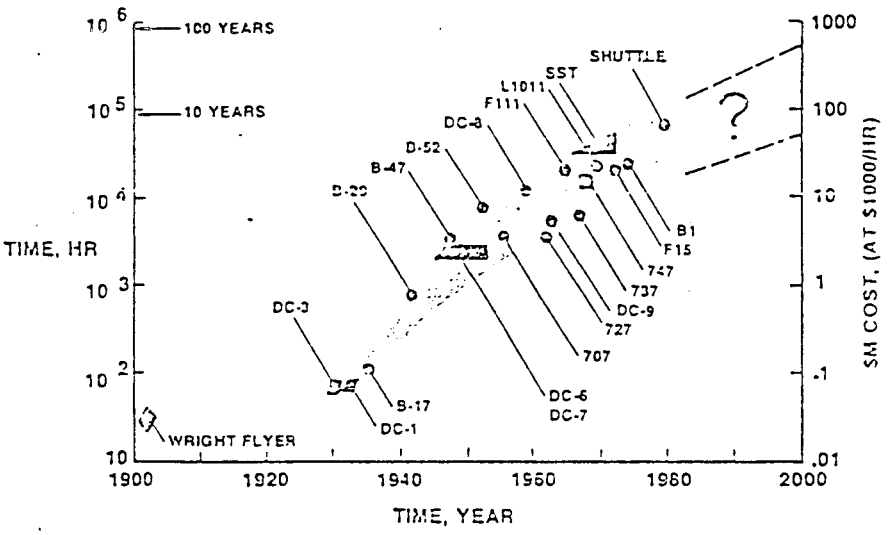

WHAT PRICE ACCURACY ?

- 10^{10} CONFIGURATIONS
- 1 MEASUREMENT/30 SECONDS
- TOTAL TIME $9.51 \cdot 10^{5}$ YEARS
- TOTAL COST $\$ 6.33 \cdot 10^{10}$

What is the Optimal Surface Pressure Distribution

(Ives, GSD)

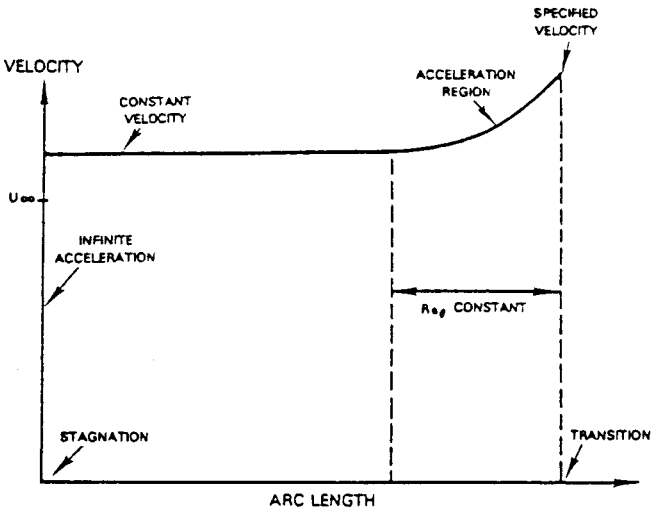

FIGURE 8. OPTIMUM VELOCITY DISTRIBUTION

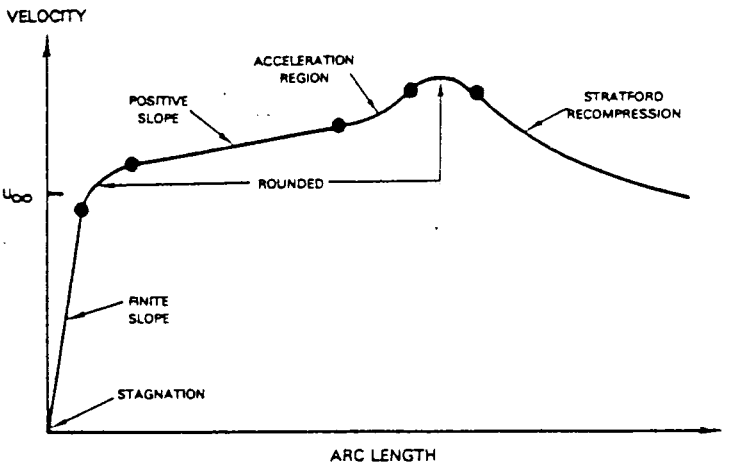

FIGURE 9. DESIGN FOR RANGE

finally, the locations of separation points should be determined from condition that

$$\rho \left\{ \left[1 - \frac{5}{2}M^2 + \frac{2-\gamma}{2} M^4 \right] (q_t + qq_s)^2 \right.$$

$$\left. + (1 - \frac{M^2}{2}) [qq_s q_t + 2q^2 q_{st} + qq_{tt} + q^2 (q_s)^2 + q^3 q_{ss}] \right\} = 0$$

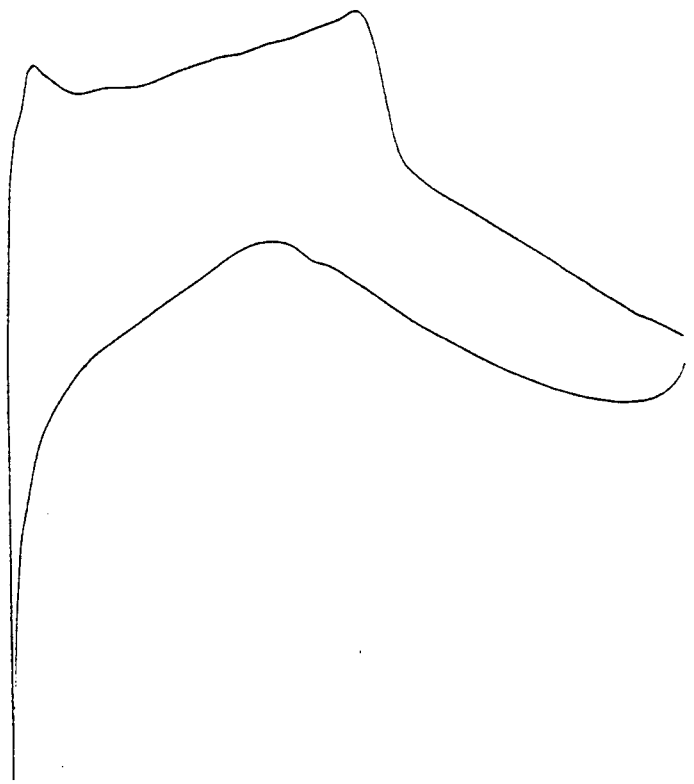

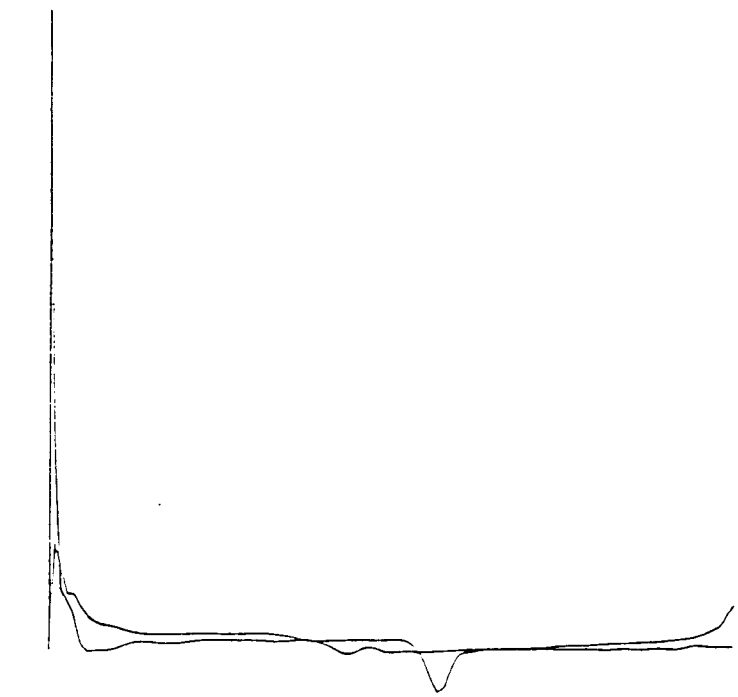

Figure 12. RAE 2822 Airfoil: surface variation of kinetic energy rate

Geometric constraints can be taken into account by putting in the library, airfoils that respect the constraints. This avoids adding a penalty function in the optimization.

Using airfoils as a set of shape functions in the optimization process produces realistic solutions at a relatively low cost. This is an easy way of modifying existing airfoils or defining new ones.

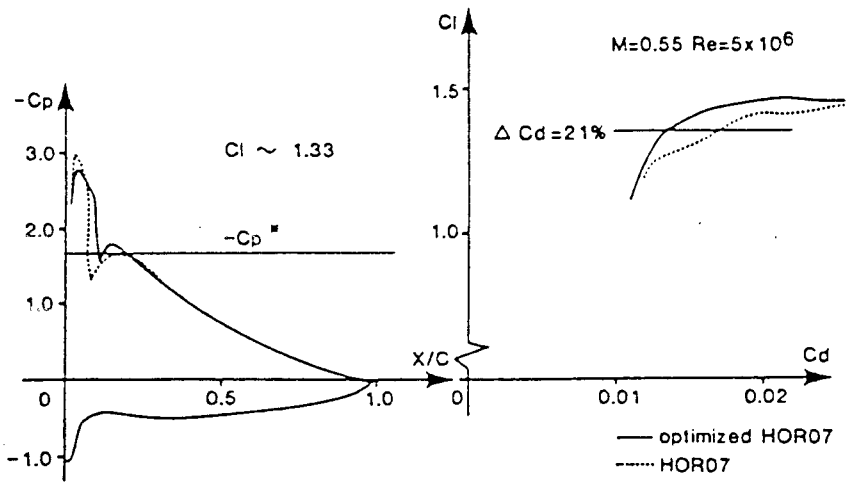

Fig. 11 — HOR07 and optimized HOR07 airfoils : experimental performances in take-off conditions

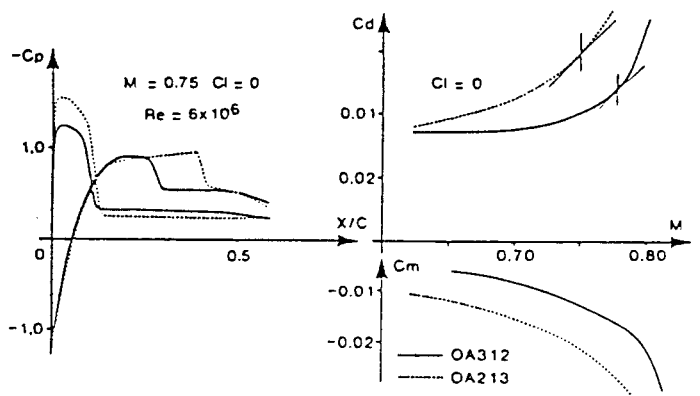

Fig. 20 — Comparison of the experimental performances of the OA213 and OA312 airfoils in advancing blade conditions

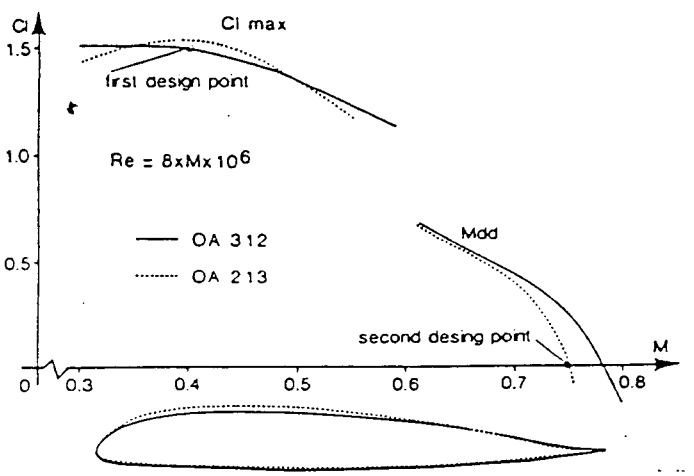

Fig. 22 — Performances of OA213 and OA312 airfoils. Experimental data

Muliphase Nozzle and Flexible Tubing Bend

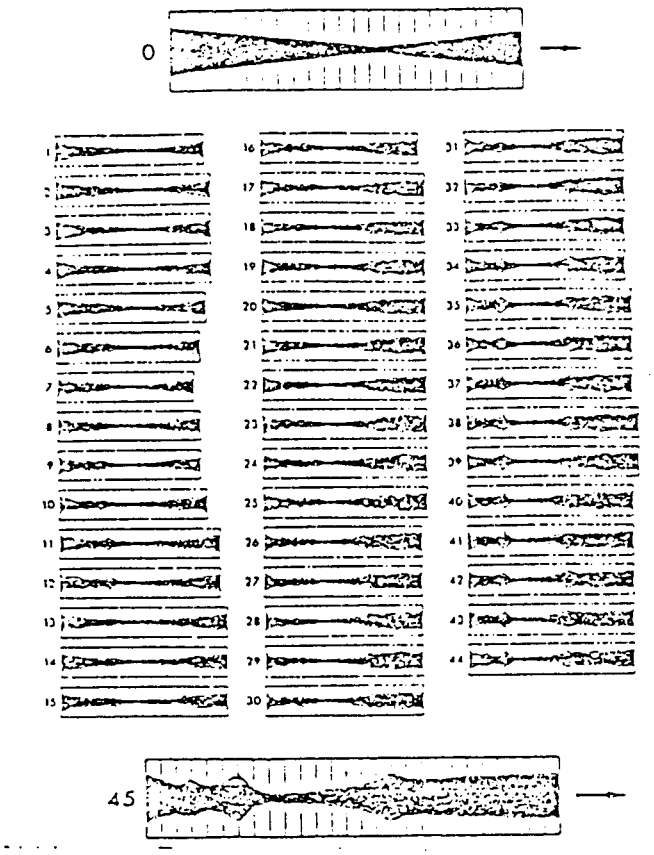

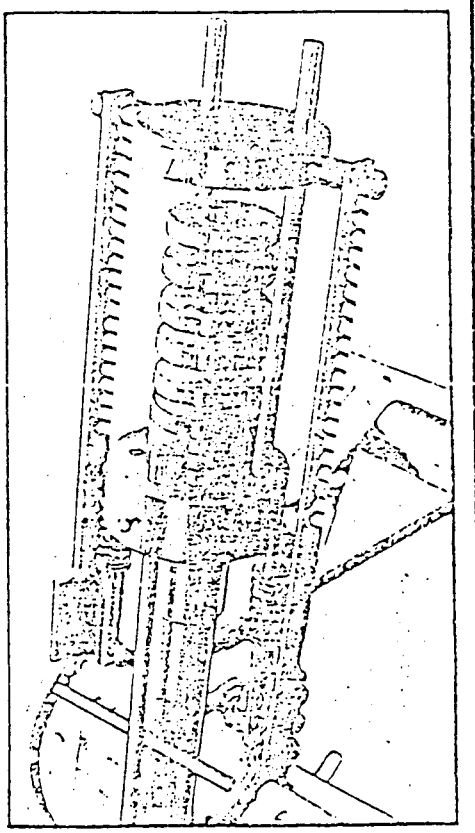

A. TWO-PHASE SUPERSONIC NOZZLE

page 6

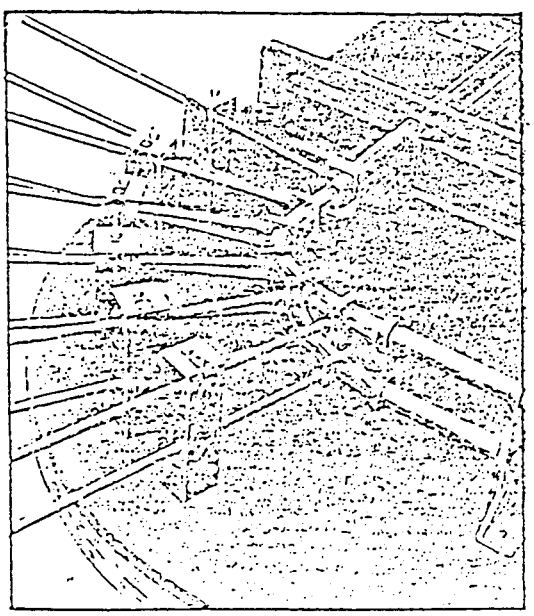

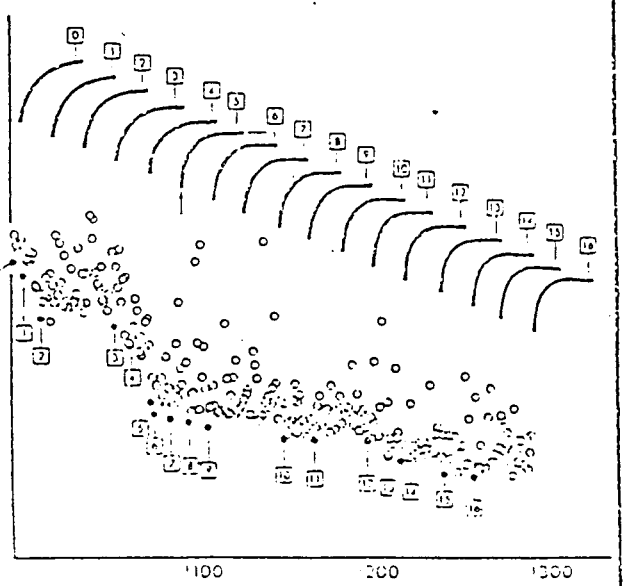

B. 90° FLEXIBLE TUBING BEND

EVOLUTION STRATEGY EXAMPLES (CONTINUED)

FIGURE 12

Multicomponent Airfoil

(Misegades & Stuff)

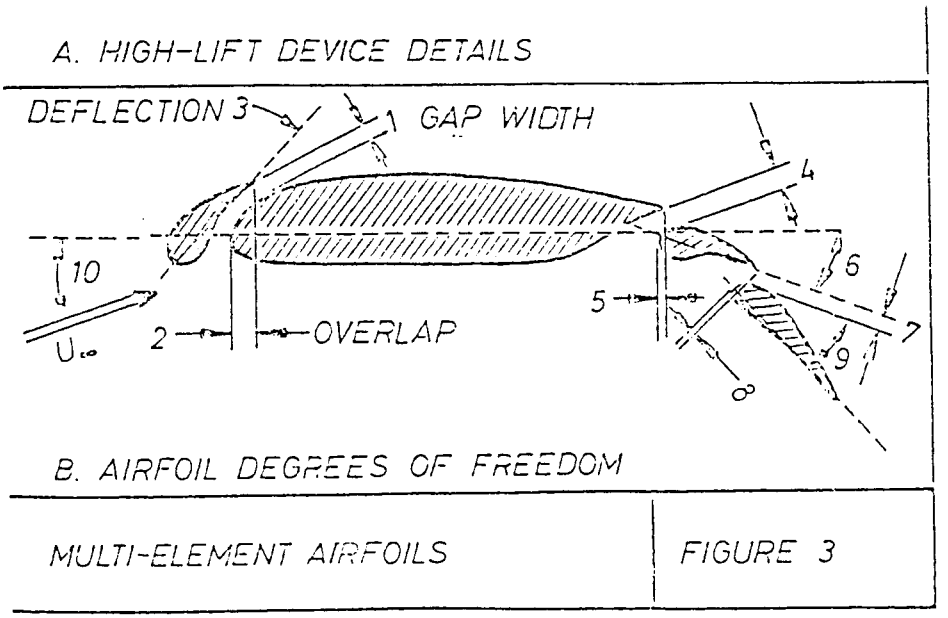

MULTI-ELEMENT AIRFOILS | FIGURE 3

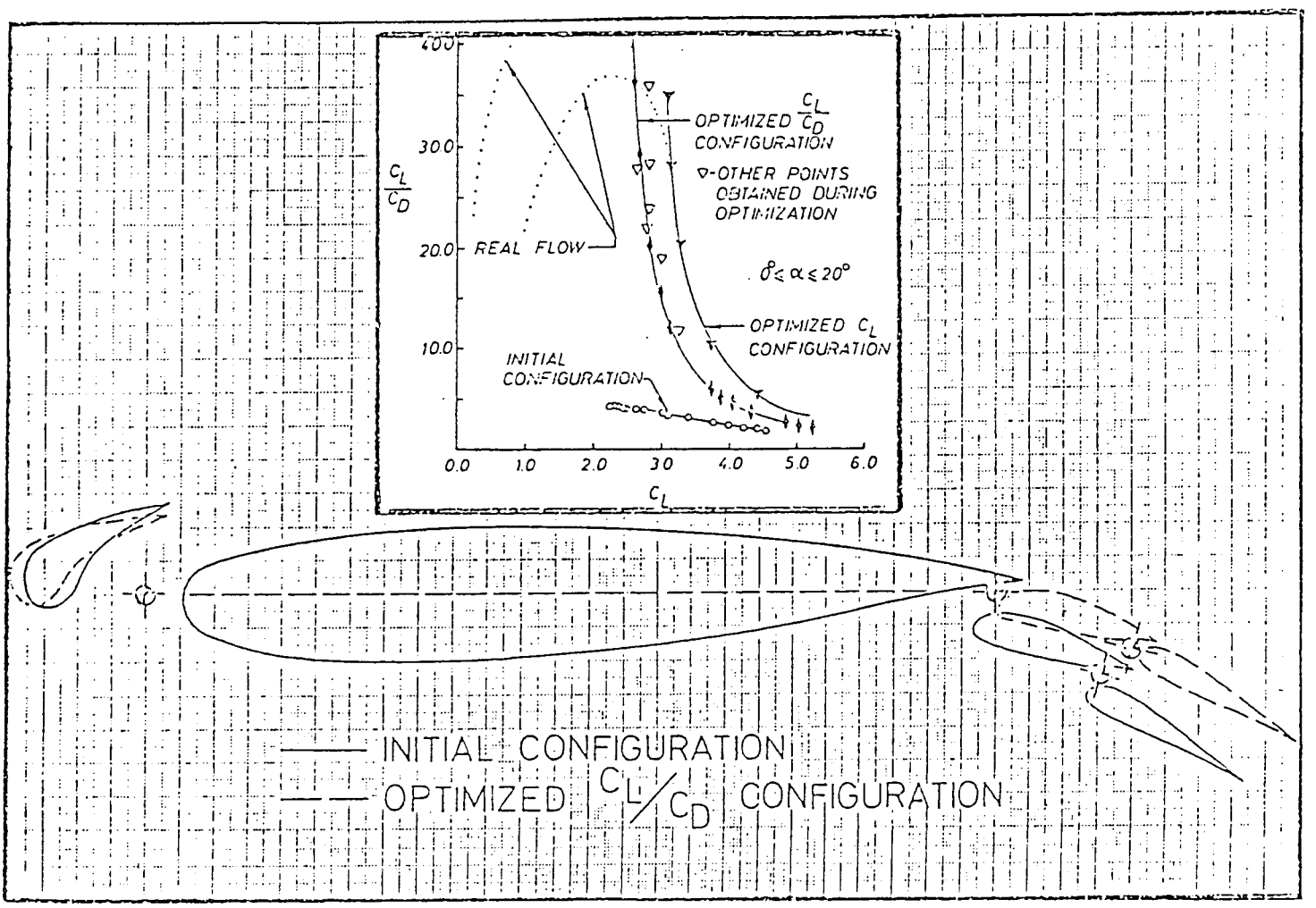

pressure distribution must inevitably be modified in order to obtain a physically meaningful wing.

Numerical Evaluation of the Integrals

In order to facilitate the numerical evaluation of the single integrals appearing in Eqs. (32) and (33), the range of integration with respect to ζ is divided into a finite number of subintervals. Assuming that $R_{\pm}(\xi,\eta)\zeta$ is constant on each subinterval, Eqs. (32) and (33) can be expressed as

$$I_s(x,y;\xi,\eta,\pm 0) = \sum_{n=0}^{K} \exp[-2R_{\pm}(\xi,\eta)\zeta_n] \times \int_{\zeta_\eta - \frac{1}{2}\Delta\zeta_{n-1}}^{\zeta_\eta + \frac{1}{2}\Delta\zeta_n} \psi_{\xi x}(x,y,0;\xi,\eta,\zeta)\,d\zeta \tag{37}$$

$$I_a(x,y;\xi,\eta,\pm 0) = \sum_{n=0}^{K} \exp[-2R_{\pm}(\xi,\eta)\zeta_n] \times \int_{\zeta_\eta - \frac{1}{2}\Delta\zeta_{n-1}}^{\zeta_\eta + \frac{1}{2}\Delta\zeta_n} \psi_{\xi z}(x,y,0;\xi,\eta,\zeta)\,d\zeta \tag{38}$$

where

$$\zeta_n = \frac{a[n/(K+1)]}{\{1-[n/(K+1)]^2\}^2}, \qquad n=0,1,2,\ldots,K \tag{39}$$

$$\Delta\zeta_n = \zeta_{n+1} - \zeta_n, \qquad \Delta\zeta_{-1} \equiv 0 \tag{40}$$

and where a is an arbitrary positive parameter and the total number of nodal points for a fixed point (ξ,η) is $K+1$.

As shown in Fig. 1, the wing surfaces are also divided into small rectangular panels of $I(2J+1)$ on each of which $\Delta u_s(x,y)$, $\Delta u_a(x,y)$, $\chi_s(x,y)$, $\chi(x,y,\pm 0)$, $R_{\pm}(x,y)$, and $\Delta w_a(x,y)$ are assumed to be constant, while $\Delta w_s(x,y)$ is assumed to vary linearly in the chordwise direction but to be constant in the other direction. These assumptions make it easy to evaluate the surface integrals numerically in Eqs. (30) and (31). The total number of unknown quantities $\Delta w_s(x^j_{i-\frac{1}{2}}, y_j)$ is $I+1$ at each span station y_j, whereas the total number of points (x^j_i, y_j) at which the known quantities such as Δu_s are defined, is I. Hence, the uniqueness of the solution can be guaranteed by imposing one additional condition, i.e., the trailing-edge closure condition of Eq. (36). The discretized form of Eq. (36) can be expressed as

$$\sum_{i=1}^{I} \tfrac{1}{2}[\Delta w_s(x^j_{i-\frac{1}{2}}, y_j) + \Delta w_s(x^j_{i+\frac{1}{2}}, y_j)](x^j_{i+\frac{1}{2}} - x^j_{i-\frac{1}{2}}) = 0 \tag{41}$$

Recalling that the perturbed flow $\Delta\phi(x,y,z)$ due to the pressure residual $\Delta C_{p\pm}(x,y/\beta)$ may be considered to be symmetrical (regardless of the presence of body) with respect to the plane $y=0$, the final expressions of Eqs. (30) and (31) in discretized form are as follows:

$$\Delta u_s(x^j_i, y_j) = \sum_{k=1}^{I+1}\sum_{m=0}^{J} \mu^s_{ijkm}\Delta w_s(x^m_{k-\frac{1}{2}}, y_m) + \chi_s(x^j_i, y_j) + \sum_{k=1}^{I}\sum_{m=0}^{J}[\nu^s_{ijkm}\chi(x^m_k, y_m, +0) + \hat{\nu}^s_{ijkm}\chi(x^m_k, y_m, -0)] \tag{42}$$

$$\Delta w_a(x^j_i, y_j) = \sum_{k=1}^{I}\sum_{m=0}^{J} \mu^a_{ijkm}\Delta u_a(x^m_k, y_m) + \sum_{k=1}^{I}\sum_{m=0}^{J}[\nu^a_{ijkm}\chi(x^m_k, y_m, +0) - \hat{\nu}^a_{ijkm}\chi(x^m_k, y_m, -0)] \tag{43}$$

where the coefficients

$$\mu^s_{ijkm},\ \mu^a_{ijkm},\ \nu^s_{ijkm},\ \nu^a_{ijkm},\ \hat{\nu}^s_{ijkm},\ \text{and}\ \hat{\nu}^a_{ijkm}$$

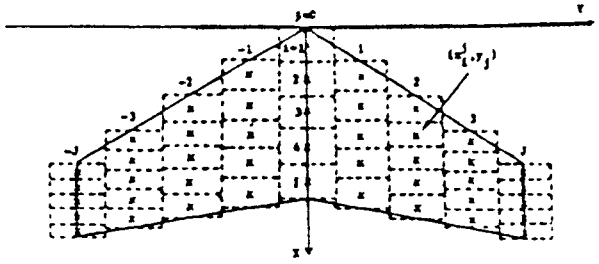

Fig. 1 Paneling of the wing surface for numerical solution of the integral equations.

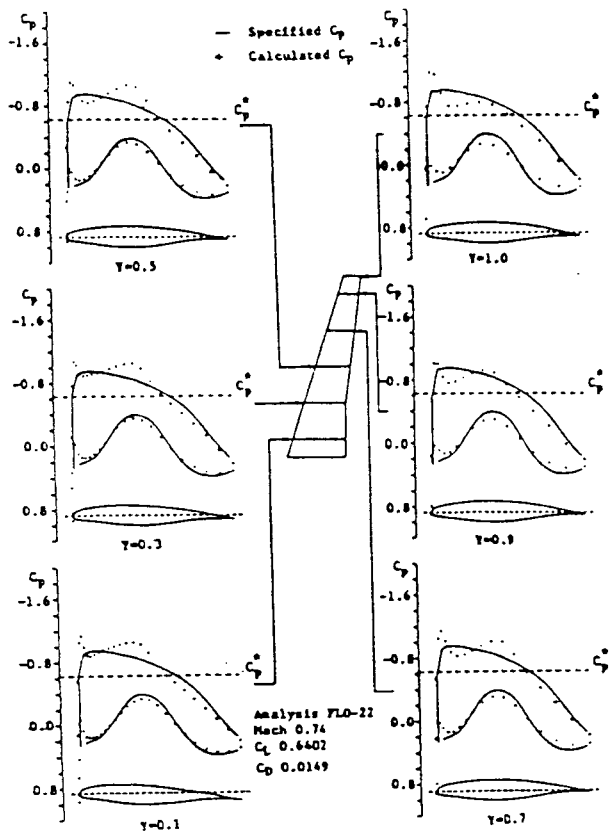

Fig. 2 Starting wing geometry and corresponding pressure distributions as well as specified (target) pressure distributions.

are the integral representations over each small panel (k,m). The full expressions are omitted here because they are lengthy and tedious.

The antisymmetric part Δw_a can be readily determined by the direct evaluation of the right-hand side of Eq. (43). On the other hand, a system of $(I+1)(J+1)$ linear equations for the symmetric part Δw_s is solved by standard techniques such as the Gaussian elimination method. Consequently, the correction Δf in the wing surface is obtained by numerically integrating Δw_s and Δw_a with respect to x.

Procedure of Iteration

The basic procedure of iteration for the wing design is described in this section. The iteration process is: 1) the flowfield is solved for an initial wing f by a direct analysis code that provides the initial pressure distribution C_p; and 2) the inverse correction code is used to obtain the value Δf of the geometric correction corresponding to the pressure difference ΔC_p between the actually computed C_p at the first step and a specified pressure distribution C_{ps}. So long as the higher-order terms ΔH, ΔQ, and ΔS are small, Δf can provide a good approximation of the exact amount of correction for the initial

MODIFIED GARABEDIAN-McFADDEN METHOD

Originally, Garabedian and McFadden developed an inverse design method suitable for transonic wing. In this method, the wing surface at each span station is unwrapped to a new surface,S(x,y) using a transformation. The surface S(x,y) is allowed to move to meet the prescribed flow quantities. The variance of the surface is governed by the equation

$$\frac{\partial S}{\partial t} + \beta_0 \frac{\partial^2 S}{\partial x \partial t} + \beta_1 \frac{\partial^2 S}{\partial y \partial t} + \beta_2 \frac{\partial^3 S}{\partial x^2 \partial t} + \beta_3 \frac{\partial^3 S}{\partial y^2 \partial t} = Q^2 - q^2 = \Delta Q^2 \qquad (1)$$

where t is pseudo-time and β_1,β_2 and β_3 are chosen to converge to the final shape as quickly and as smoothly as possible. Q is defined as the specified target pressure distribution in terms of velocities and q is the calculated speed from the flow solver.

Malone et. al. suggested the following modification. Instead of applying eq (1) in the transformed coordinate they applied it directly in the physical domain with the modified equation

$$\beta_0 \frac{\partial Z}{\partial t} + \beta_1 \frac{\partial^2 Z}{\partial x \partial t} + \beta_2 \frac{\partial^3 Z}{\partial x^2 \partial t} = Q^2 - q^2 = \Delta Q^2 \qquad (2)$$

where Z is the body surface and is a function of x only.

First, discretizing the time terms we have

$$\frac{\beta_0}{\Delta t}\Delta Z + \frac{\beta_1 \partial \Delta Z}{\Delta t \ \partial x} + \frac{\beta_2 \partial^2 \Delta Z}{\Delta t \ \partial x^2} = \Delta Q^2 \qquad (3)$$

where $\Delta Z = Z - Z^{old}$

Because we use the pseudo-time to evolve the equation, we can choose Δt to be equal to 1 for convenience. In order to apply eq (3) to both the upper and lower surfaces, ΔZ should be negative for the lower surface and positive for the upper surface. Introducing β_3 as follows, we can solve the problem.

$\beta_3 = -1$ for lower surface

$\beta_3 = 1$ for upper surface

$$\beta_0 \Delta Z + \beta_1 \frac{\partial \Delta Z}{\partial x} + \beta_2 \frac{\partial^2 \Delta Z}{\partial x^2} = \beta_3 \Delta Q^2 \qquad (4)$$

The spatial derivatives are approximated with upwind differencing for the first derivative term and central differencing for the 2nd derivative term. The upwind differencing is used for introducing the artificial dissipation into the equation to eliminate the well known even-odd decoupling when using central differencing only.

The final form of the discretized equation is given by

$$A_i \Delta Z_{i+1} + B_i \Delta Z_i + C_i \Delta Z_{i-1} = \Delta Q^2 \qquad (5)$$

where the coefficients for the upper surface are given as

$$A_i = \frac{2\beta_2}{(x_{i+1} - x_{i-1})(x_i - x_{i-1})} - \frac{\beta_2}{x_i - x_{i-1}}$$

$$B_i = \beta_0 + \frac{\beta_1}{(x_i - x_{i+1})} - \frac{2\beta_2}{(x_i - x_{i+1})(x_{i-1} - x_i)}$$

$$C_i = \frac{2\beta_2}{(x_{i+1} - x_{i-1})(x_{i+1} - x_i)} \qquad (6)$$

For the lower surface, they are given by

$$A_i = \frac{2\beta_2}{(x_i - x_{i-1})(x_{i+1} - x_{i-1})}$$

$$B_i = \beta_0 - \frac{\beta_1}{x_{i+1} - x_i} + \frac{2\beta_2}{(x_i - x_{i-1})(x_{i+1} - x_i)}$$

$$B_i = \frac{\beta_1}{x_{i+1} - x_i} + \frac{2\beta_2}{(x_i - x_{i-1})(x_{i+1} - x_{i-1})} \qquad (7)$$

Since we treat the upper and lower surfaces differently, special care should be exercised at the leading and the trailing edges of the airfoil. The location of trailing edge must remain fixed or the problem will be indeterminate, while the leading edge is allowed to move and the movement is set to the average of the movements of the neighboring two points.

Thus,

$$-\Delta Z_{i+1} + 2\,\Delta Z_i - \Delta Z_{i-1} = 0 \qquad (8)$$

which gives

$$A_i = -0.5$$

$$B_i = 1.0$$

$$C_i = -0.5 \qquad (9)$$

The resulting matrix is tridiagonal,which allows us to solve it using Thomas Algorithm.

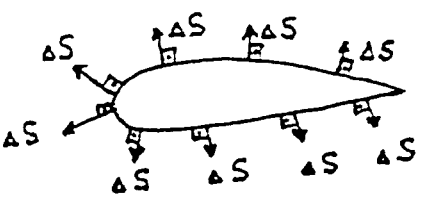

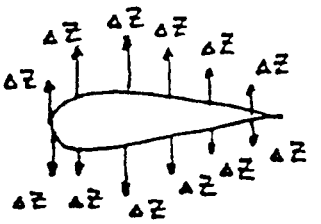

7. REFERENCES

1. Malone, J.B., Vadyak, J., and Sankar, L.N. A Technique For The Inverse Aerodynamic Design Of Nacelles and Wing Configurations . AIAA Paper No. 85-4096, October, 1985.

2. Garabedian, P. and McFadden, G. Design Of Supercritical Swept Wings . AIAA Journal, Vol. 20, No. 3, March, 1982, pp 289-291.

3. Chin, W. Class Of Shockfree Airfoils Producing The Same Surface Pressure . Journal of Aircraft, Vol 17, No. 4, April, 1980, pp 286-288.

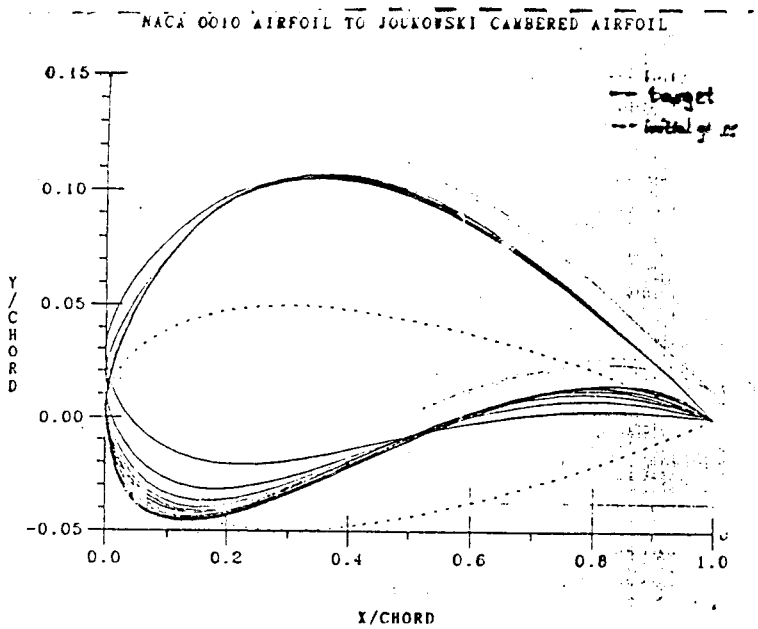

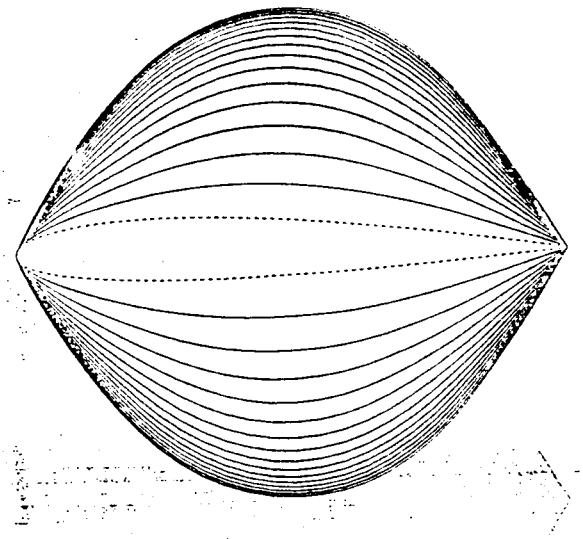

FIGURE 6
NACA 2410 PROFILE EVOLUTION INTO A CYLINDER

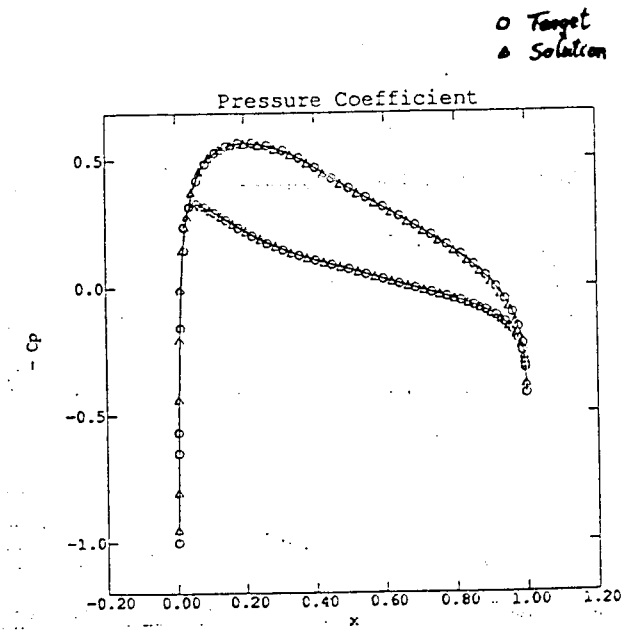

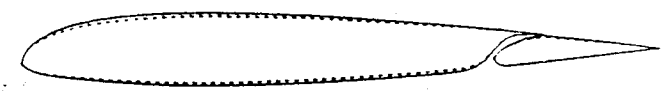

Airfoil and a flap

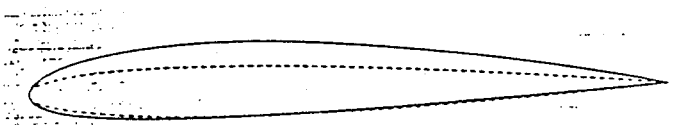

NACA 0008 → NACA 4212

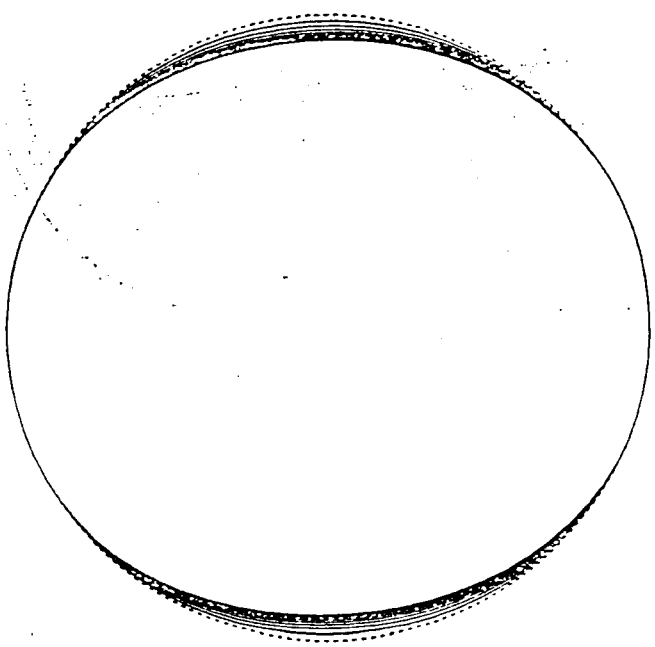

FULL POTENTIAL EQUATION: USE SURFACE Cp FROM A PERFECT CIRCLE IN INCOMPRESSIBLE FLOW TO GET A SHAPE AT $M_\infty = 0.4$.

FIG(5) INITIAL AND FINAL AREA VALUES'S

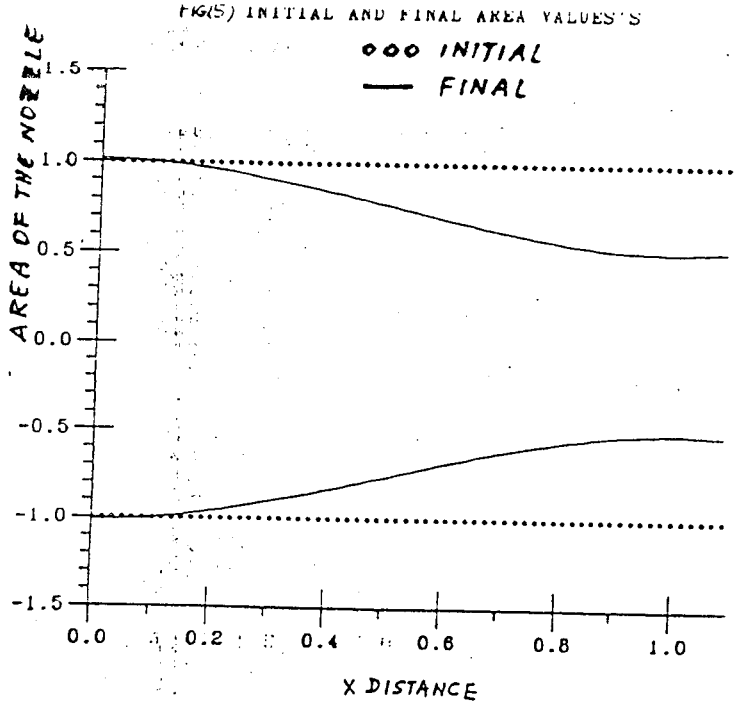

FIG.(6) EXACT AND DESIGN MACH NUMBERS

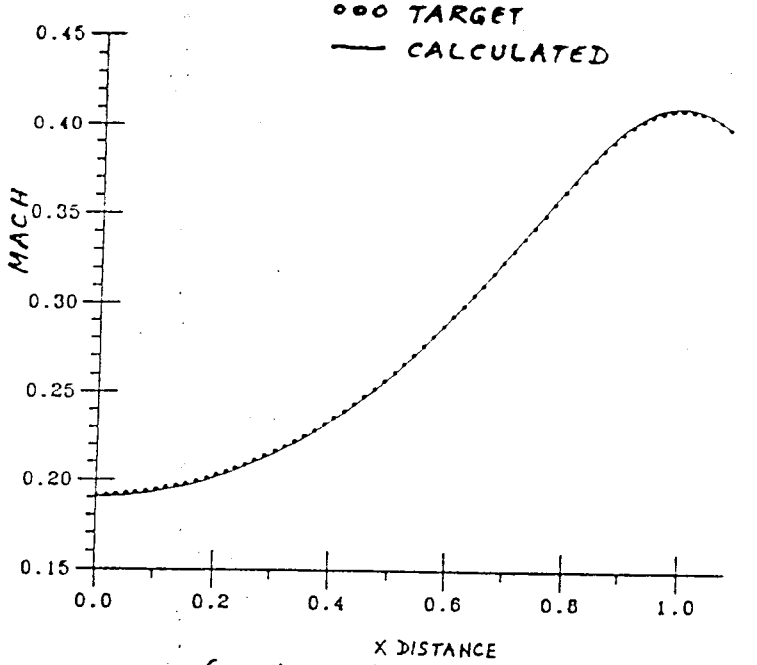

QUASI-ONEDIMENSIONAL EULER CODE (B-W) USED IN A NOZZLE DESIGN

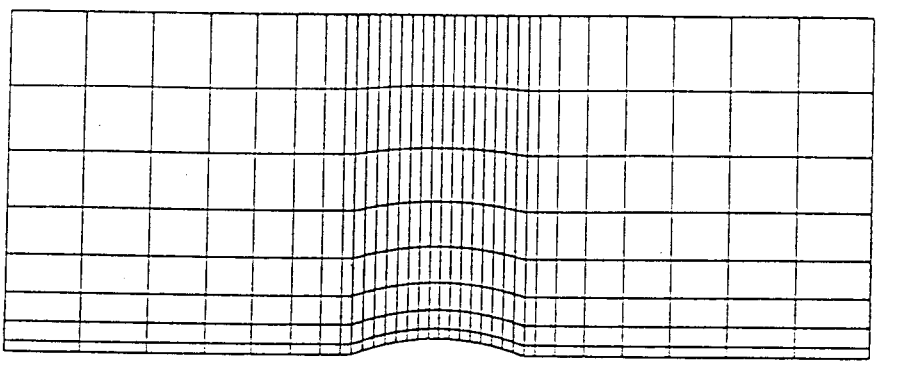

ORIGINAL SHAPE HAVING A BUMP

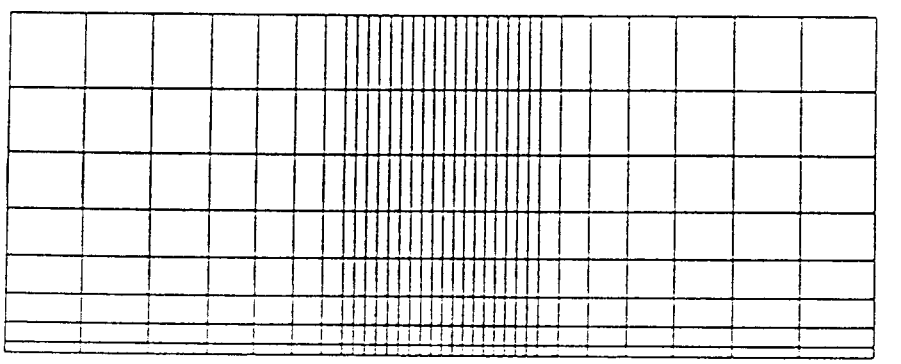

FINAL SHAPE FOR A UNIFORM FLOW WITH $M=0.5$ OBTAINED BY USING JAMESON'S TYPE ALGORITHM FOR EULER EQUATIONS OF GASDYNAMICS

CP VS. X EQUIVALENT AIRFOILS ALPHA=3.9.3 DEGREES

EQUIVALENT AIRFOIL NACA 0014 ALPHA=3 DEGREES

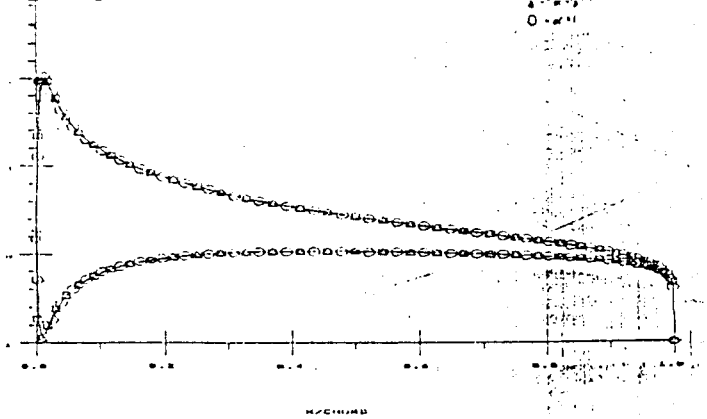

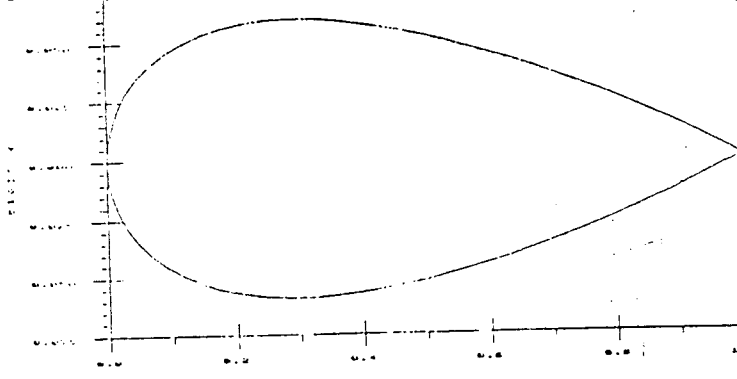

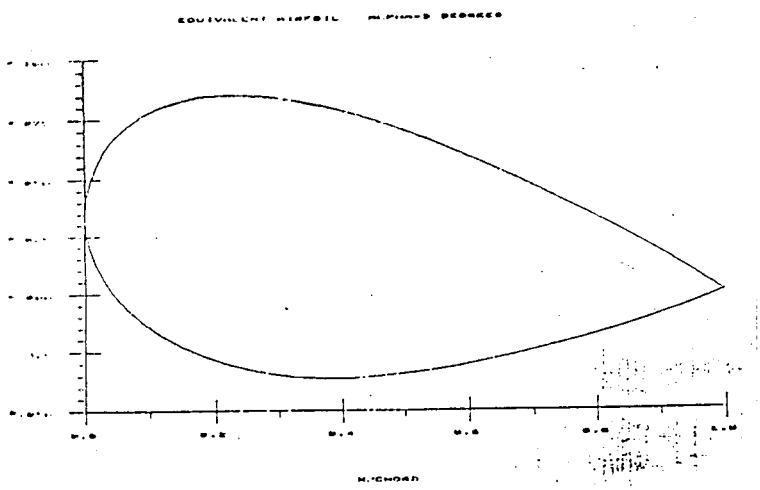

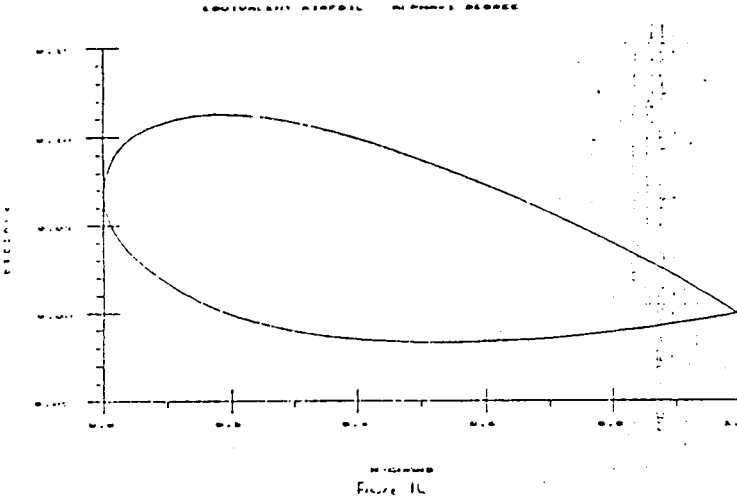

NOZZLE AREA PER ITERATION

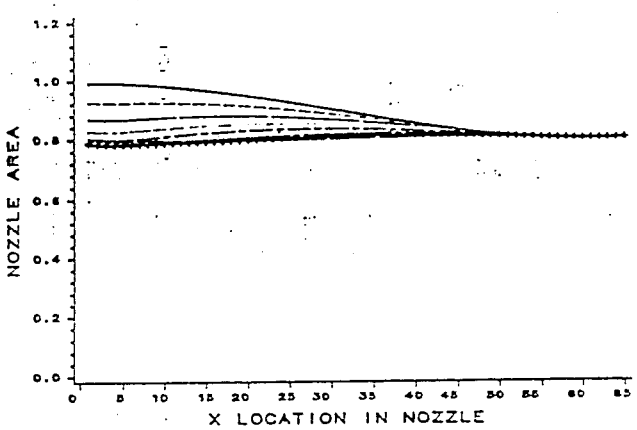

MACH NUMBER IN NOZZLE PER ITERATION

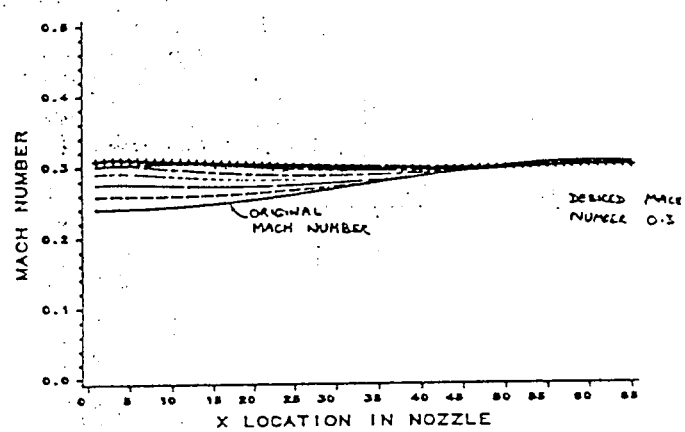

Engineering Notes

ENGINEERING NOTES are short manuscripts describing new developments or important results of a preliminary nature. These Notes cannot exceed 6 manuscript pages and 3 figures; a page of text may be substituted for a figure and vice versa. After informal review by the editors, they may be published within a few months of the date of receipt. Style requirements are the same as for regular contributions (see inside back cover).

$$u = \frac{\partial \psi}{\partial y} \; ; \qquad v = -\frac{\partial \psi}{\partial x}$$

An Inverse Boundary Element Method for Single Component Airfoil Design

Erkki Soinne* and Seppo Laine†
Helsinki University of Technology
Espoo, Finland

Nomenclature

a,b	= $\xi-$ and $\eta-$coordinates of control point
c	= airfoil chord
d	= half of the element length
k,ϵ,μ	= parameters defining Karman-Trefftz airfoil
K_{ij}	= element of the influence coefficient matrix
r	= distance from a vortex density contribution to a control point
s	= curvilinear coordinate along the airfoil contour
S	= airfoil perimeter
U_0	= freestream velocity
x,y	= Cartesian coordinates
α	= angle between the x-axis and the freestream
γ	= strength of vortex sheet
ξ,η	= element local Cartesian coordinates
ψ	= stream function
ψ_S	= value of stream function along the airfoil contour

Introduction

An important task in airfoil design is the determination of the airfoil contour corresponding to a prescribed velocity distribution. In the present study, this design problem, also called inverse problem, is considered for single component airfoils in inviscid, incompressible flow. There are several possible approaches to solve the inverse problem; here the stream function method is utilized. In this method, an integral equation is formed for the stream function describing the flow.

The stream function method has been used by several researchers in connection with problems of both analysis and design. Oellers[1] used the method in the analysis of flow around cascades in 1962. Ormsbee and Chen[2] presented a design method in 1972 using a constant strength vorticity element. Later on, variants of this method were developed by Mavriplis,[3] and Kennedy and Marsden.[4]

In this Note, a new method is developed which utilizes a straight line element with linearly varying vortex density. Here the control points are placed exactly on the airfoil contour, and therefore a separate determination of the contour coordinates is eliminated. This makes the new method simpler than the previous approaches.

Received Oct. 6, 1984; revision received Jan. 10, 1985.

*Research Engineer; presently at Saab-Scania Aerospace Company, Linköping, Sweden.
†Professor of Aeronautical Engineering. Member AIAA.

Inverse Calculation Method

Using the stream function method the airfoil in two-dimensional potential flow is replaced by a vortex sheet on the airfoil surface. To satisfy the condition that there should be no flow through the airfoil surface, the total stream function

$$\psi = U_0(y\cos\alpha - x\sin\alpha) + 1/2\pi \oint_S \gamma(s)\ln\left(\frac{r}{c}\right)ds \qquad (1)$$

must be constant along the whole surface. For a closed airfoil, the velocity distribution is equal to the vortex distribution.

In the boundary element approach, the integral equation is solved by dividing the vortex sheet into boundary elements that may have varying vortex density. In collocation methods, the values of vortex density are expressed at nodes j and the integral equation is satisfied at an equal number of collocation points i. The integral equation can now be replaced at a specified collocation or control point i by the algebraic equation

$$\psi_S = U_0(y_i\cos\alpha - x_i\sin\alpha) - \sum_j K_{ij}\gamma_j \qquad (2)$$

where K_{ij} is the influence coefficient of the vortex density γ_j at node j. The expression for the y coordinate at control point i can be written

$$y_i = \frac{1}{U_0\cos\alpha}\left[\psi_S + \sum_j K_{ij}\gamma_j\right] + x_i\tan\alpha \qquad (3)$$

This equation, which presents a formula to solve iteratively the y coordinates of the control points, is common to many inverse calculation methods.

When an element with a constant vortex density is used, the control point is usually placed in the middle of the element. The control point then falls inside the airfoil contour with the element endpoints being on the contour. This raises the problem of determining the relative location of the airfoil contour with respect to the derived control points. Chen[2] utilized a third order Lagrangian interpolation to establish the relation between the airfoil contour and the control points. Kennedy and Marsden[4] preferred a method where the pseudo-control

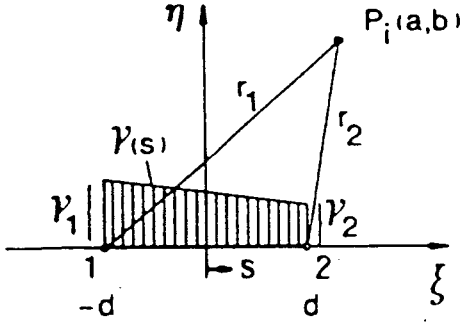

Fig. 1 Linear vortex element in local (ξ,η) coordinate system. P_i is an arbitrary control point.

point at the airfoil trailing edge is used as a starting point for straight line segments passing through the control points. The method is fairly simple but, according to them, contains the risk of producing a sawtooth-shaped airfoil, since small errors can propagate from the trailing edge to the leading edge.

In the present method these difficulties are avoided by using a straight line element with linearly varying vortex density. Both the nodes and the control points are placed at the element endpoints, exactly on the airfoil contour. The influence coefficients of a linear element can be derived by analytic integration.[5] Using the notation of Fig. 1, the general expressions for the influence coefficients of the left-and right-hand nodal vorticities, γ_1 and γ_2, of an element are of the form

$$K'_{i1} = -1/4\pi\left\{(a+d)\ln r_1 - (a-d)\ln r_2 - 2d + b\left[\overline{\arctan}\frac{a+d}{b} - \overline{\arctan}\frac{a-d}{b}\right]\right\} + 1/4\pi\left\{\frac{a^2-b^2-d^2}{2d}[\ln r_1 - \ln r_2] - a + ab/d\left[\overline{\arctan}\frac{a+d}{b} - \overline{\arctan}\frac{a-d}{b}\right]\right\} \quad (4)$$

$$K'_{i2} = -1/4\pi\left\{(a+d)\ln r_1 - (a-d)\ln r_2 - 2d + b\left[\overline{\arctan}\frac{a+d}{b} - \overline{\arctan}\frac{a-d}{b}\right]\right\} - 1/4\pi\left\{\frac{a^2-b^2-d^2}{2d}[\ln r_1 - \ln r_2] - a + ab/d\left[\overline{\arctan}\frac{a+d}{b} - \overline{\arctan}\frac{a-d}{b}\right]\right\} \quad (5)$$

where definitions

$$r_1 = \sqrt{(a+d)^2 + b^2} \quad (6)$$

$$r_2 = \sqrt{(a-d)^2 + b^2} \quad (7)$$

have been used. Equations (4) and (5) are valid outside the element. When the control point coincides with either of the nodes of the element, the equations reduce to the forms:

$$K'_{11} = K'_{22} = d/4\pi[3 - 2\ln(2d)] \quad (8)$$

$$K'_{12} = K'_{21} = d/4\pi[1 - 2\ln(2d)] \quad (9)$$

With the element influence coefficients of Eqs. (4), (5), (8) and (9), the global influence coefficients, K_{ij}, can be assembled without difficulty.

The y coordinates of the airfoil contour are solved iteratively through Eq. (3) starting from an arbitrary airfoil. During the iteration, the global influence coefficients K_{ij} are calculated for the airfoil from the previous iteration step.

Examples

An example of the convergence of the present design method is given in Fig. 2. This shows the specified velocity distributions on the upper and lower airfoil surfaces, the initial airfoil for starting the iteration, the final airfoil contour after ten iteration cycles and the corresponding velocity distributions. The required computing time is approximately 3.5 s CPU time per iteration cycle on a DEC-20 computer.

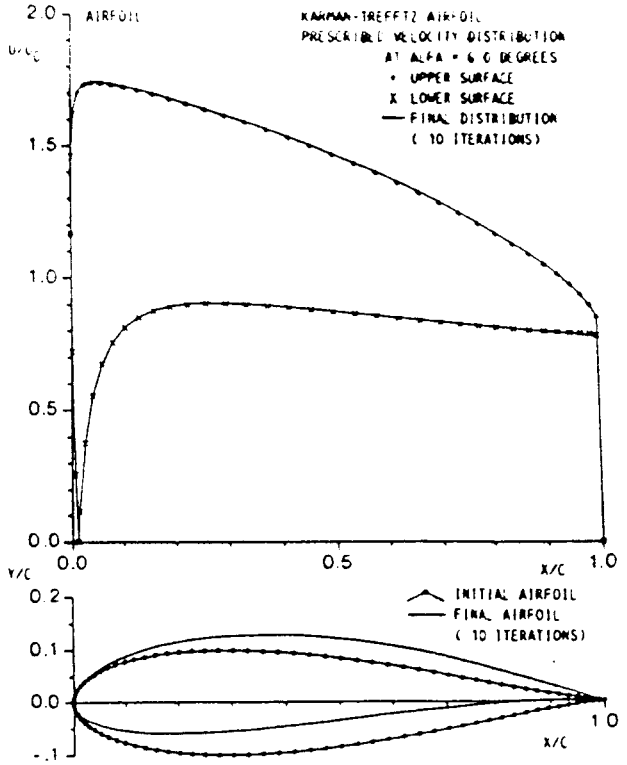

Fig. 2 Determination of the contour of a Kármán-Trefftz airfoil from the prescribed velocity distribution (75 nodes).

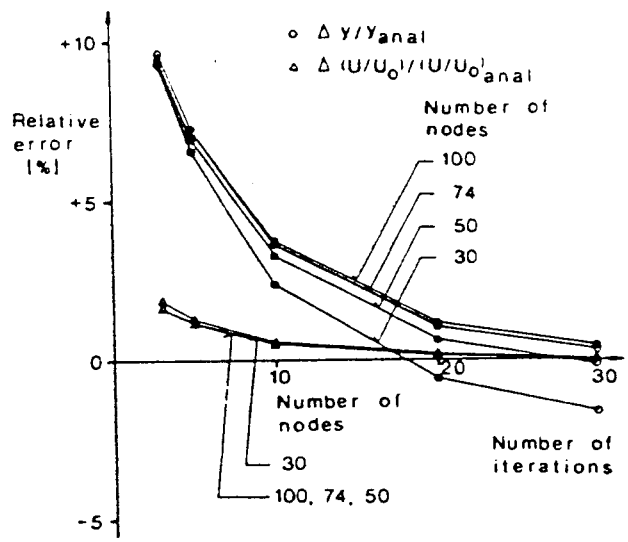

Fig. 3 Relative error of the dimensionless y-coordinate and velocity on the upper surface of a Kármán-Trefftz airfoil at the node at $x/c = 0.4$. The final airfoil has parameter values $\epsilon = 0.13$, $k = 1.95$ and $\mu = 0.1$. The initial airfoil has parameter values $\epsilon = 0.15$, $k = 1.9$ and $\mu = 0$.

Previous researchers have used the velocity distribution of the final airfoil as a measure of the convergence of design methods. However, in the opinion of the authors this gives a distorted view of the phenomenon because the element-specific error is not taken into account. The convergence of the velocity and y-coordinate value on the upper surface of the Kármán-Trefftz airfoil of Fig. 2 is shown in Fig. 3 for differing numbers of nodes used. The velocity error moves clearly toward zero as is required in the iteration sheme, whereas the element-specific error causes the $y-$coordinate error to move towards a level other than zero. The final airfoil would probably be too thin in all of the four cases, although the $y-$coordinate error has not changed sign at the two highest numbers of nodes.

Reference 5 includes a computer program for the inverse and analysis problems as well as results of further numerical tests.

Conclusions

An inverse boundary element method for airfoil design has been developed using a straight line element with linearly varying vortex density. The control points are placed exactly on the airfoil contour, making any interpolation or smoothing of the contour during the iteration unnecessary. The new method is more straight-forward than the previous approaches.

It has been shown that when the convergence of a design method is studied, the element-specific error must be taken into account.

Acknowledgments

This work has been supported by the Research Council for Technology of the Academy of Finland.

References

[1]Oeliers, H. J., "Die inkompressible Potentialströmung in der ebenen Gitterstufe," *Jahrbuch 1962 der Wissenschaftlichen Gesellschaft für Luft- und Raumfahrt e. V., Cologne*, pp. 349-353.

[2]Ormsbee, A. I., and Chen, A. W., "Multiple Element Airfoils Optimized for Maximum Lift Coefficient," *AIAA Journal*, Vol. 10, Dec. 1972, pp. 1620-1624.

[3]Mavriplis, F., "Aerodynamic Predicton and Design Methods of Aircraft High Lift Systems," *Proceedings of the Aerodynamics Seminar*, National Research Council of Canada, May 1974, pp. 1-26.

[4]Kennedy, J. L., and Marsden, D. J., "A Potential Flow Design Method for Multicomponent Airfoil Sections," *Journal of Aircraft*, Vol. 15, Jan. 1978, pp. 47-52.

[5]Soinne, E., "Design of Single Component Airfoils Using an Inverse Boundary Element Method," Helsinki University of Technology, Laboratory of Aerodynamics, Otaniemi, Rept. 83-A2, 1983.

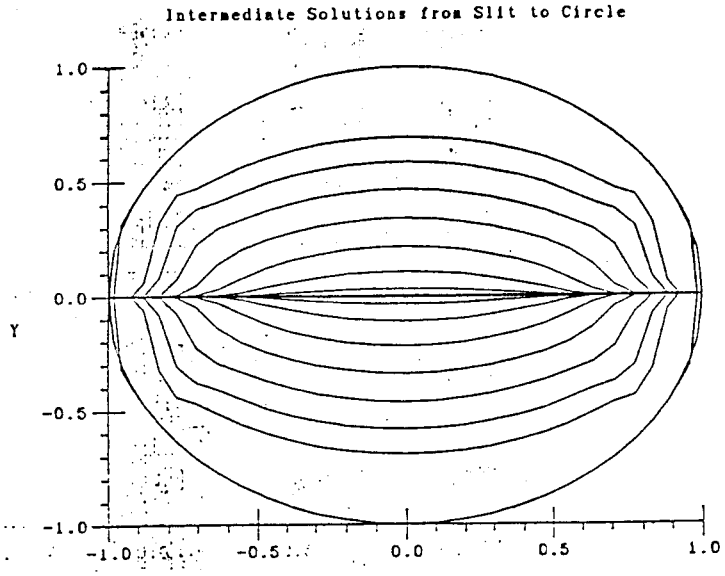

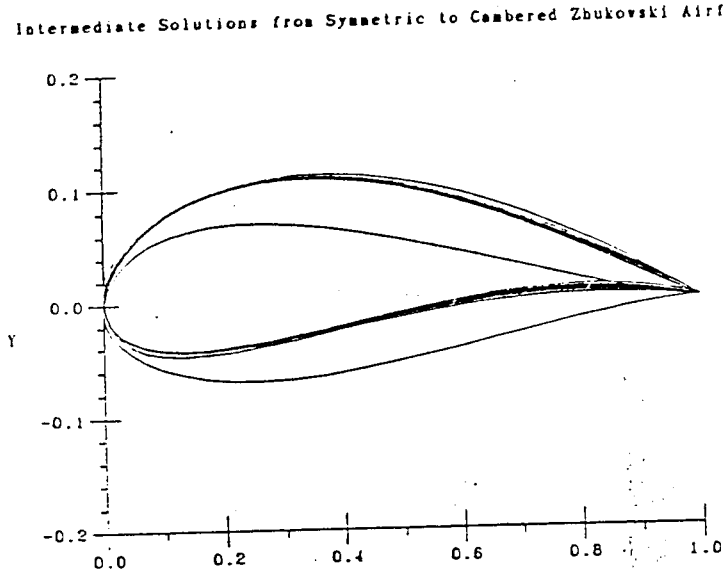

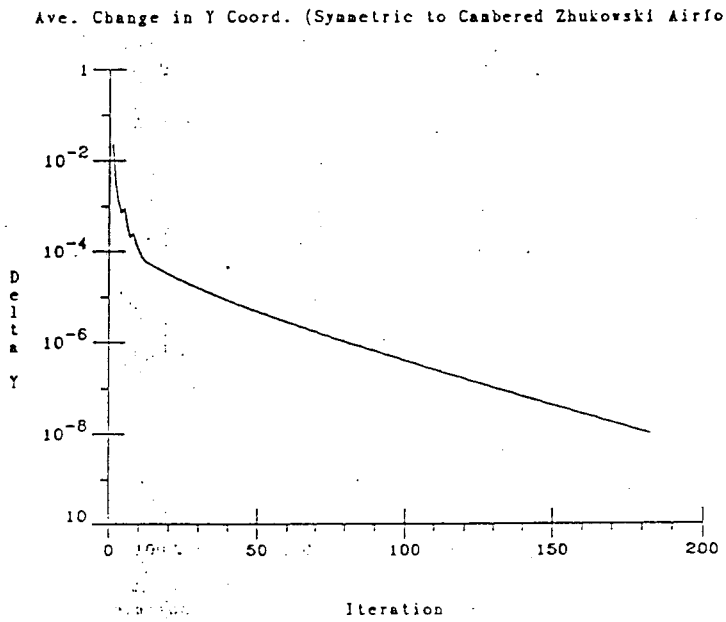

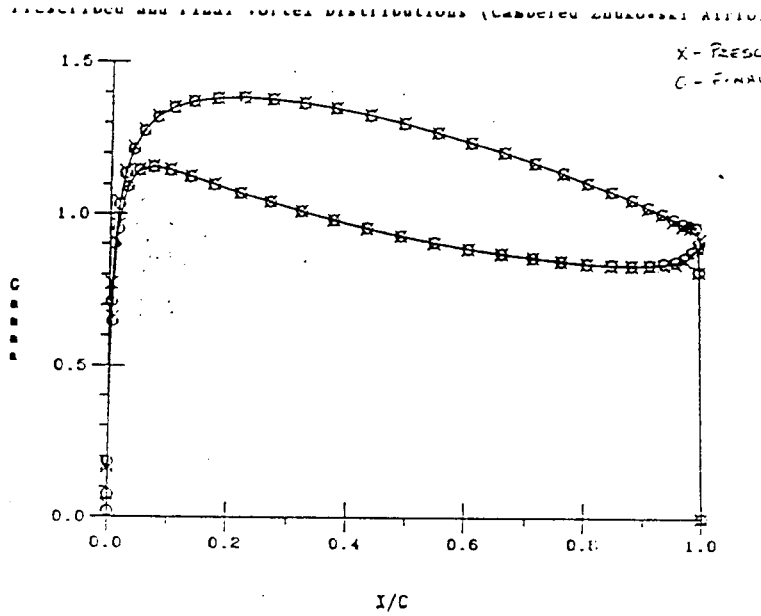

STREAMFUNCTION METHODS FOR DUCTS, CHANNELS & CASCADES

1. INTRODUCTION

In the theory of fluid motion, there are two general types of boundary value problems: (1) the direct problem, in which the distribution of velocity is determined for a prescribed shape of boundary, and (2) the inverse problem, in which the shape of the boundary is determined for a prescribed distribution of velocity along it. The direct problem is an analysis problem; the inverse problem is a design problem. This report is concerned with the inverse design problem for steady potential flow through ducts.

An aerodynamic approach to an inverse design of flow fields is very attractactive, because the inverse method starts with a prescribed velocity distribution on the boundary and generates a body profile which will produce the intended velocity distribution. Through the control of the velocity distribution on the boundaries : (1) boundary-layer separation losses can be avoided by prescribed velocity in the direction of flow that do not decelerate rapidly enough to cause separation, (2) shock losses in compressible flow and cavitation in incompressible flow can be avoided by prescribed velocities that do not exceed certain maximum values dictated by these phenomena, and (3) for compressible flow in ducts, the desired flow rate can be assured by prescribed velocities that do not result in premature choked flow.

Several methods of channel design have been developed. But all these methods can be applied to a particular problem, such as accelerating elbows or symmetrical channels with contracting or expanding walls for incompressible or linearized compressible flow.

(1) Stanitz, John D.: Design of Two-Dimensional Channels with Prescribed Velocity Distributions Along the Channel Walls. Part I - Relaxation Solutions. NACA TN 2593, January 1952. (Superseded by NACA TR 1115.)

(2) Stanitz, John D.: Design of Two-Dimensional Channels with Prescribed Velocity Distributions Along the Channel Walls. Part II - Solution by Green's Function. NACA TN 2595, January 1952. (Superseded by NACA TR 1115.)

(3) Stanitz, John D., and Sheldrake, Leonard J.: Application of a Channel Design Method to High-Solidity Cascades and Tests of an Impulse Cascade with 90° of Turning. NACA TN 2652, March 1952. (Superseded by NACA TR 1116.)

(4) Stanitz, John D., Osborn, Walter M., and Mizisin, John: An Experimental Investigation of Secondary Flow in an Accelerating, Rectangular Elbow with 90° of Turning. NACA TN 3015, October 1953.

(5) Stanitz, John D.: Aerodynamic Design of Efficient Two-Dimensional Channels. ASME Transactions, vol. 75, no. 7, October 1953.

(6) Stanitz, John D.: General Design Method for Three-Dimensional, Potential Flow Fields. Part I - Theory. NASA CR 3288, August 1980.

(7) Stanitz, John D.: General Design Method for Three-Dimensional, Potential Flow Fields. Part II - Computer Program DIN3D1 for Simple, Unbranched Ducts. NASA CR 3926, September 1985.

(8) Clebsch, A.: Über eine allgemeine Transformation der hydrodynamischen Gleichungen. Journal für Mathematik, Bd. LIV, Heft 4, 1857.

(9) Yih, Chia-Shun: Stream Functions in Three-Dimensional Flows. La Houille Blanche, vol. 12, no. 3, July-Aug. 1957.

(10) Yang, Tah-teh; Hudson, William G., and Nelson, Carl D.: Design and Experimental Performance of Short Curved Wall Diffusers with Axial Symmetry Utilizing Slot Suction. NASA CR 2209, 1973.

(11) Stanitz, John D.: Compressible Inviscid Flow [illegible]

Outline of method. The inverse method for 3-dimensional channel design is not unlike that for the 2-dimensional case, although rather more complex. For 3-dimensional design, the problem is solved in φ,ψ,η-space where the distribution of q on the boundary is known from equation (3) and from the specified distribution of q as a function of arc length s along each boundary streamline (constant ψ,η). A governing differential equation for the distribution of ln q in φ,ψ,η-space is solved by finite difference methods; the distribution of nine direction cosines, associated with the three unit vectors $\bar{e}_1$, $\bar{e}_2$ and $\bar{e}_3$, are determined from the spatial distribution of ln q; and the distributions of x, y and z in φ,ψ,η-space are determined from the distributions of ln q and the direction cosines.

Physical x,y,z space. - The flow field at a point in physical x,y,z space has two stream surfaces of constant ψ and η, respectively, that intersect the potential surface at 90° and intersect one another at an angle Θ measured on the potential surface (ref. 1). The directions of these three intersections are given by the unit vectors $\bar{e}_1$, $\bar{e}_2$, and $\bar{e}_3$, each defined by its direction cosines cos α, cos β, and cos γ. Differential lengths along the intersections are given by ds, dm, and dn, as shown in the following figure.

The velocity vector $\bar{q}$ ($\bar{e}_1 q$) is tangent to the intersection of the ψ and η stream surfaces so that $\bar{q}$ is normal to the potential surface φ, and ψ and η are constant along the streamline.

the same shape as the upstream boundary configuration in x,y,z space, provided that the stream surfaces ψ and η at the upstream boundary are defined by lines of constant y and z, respectively (ref. 1). Lines of constant ψ and η (paired values) on the lateral boundary are streamlines, and the velocity vector $\bar{q}$ is everywhere parallel to the φ axis. The rectangular grid resulting from the intersections of surfaces of constant φ, ψ, η.

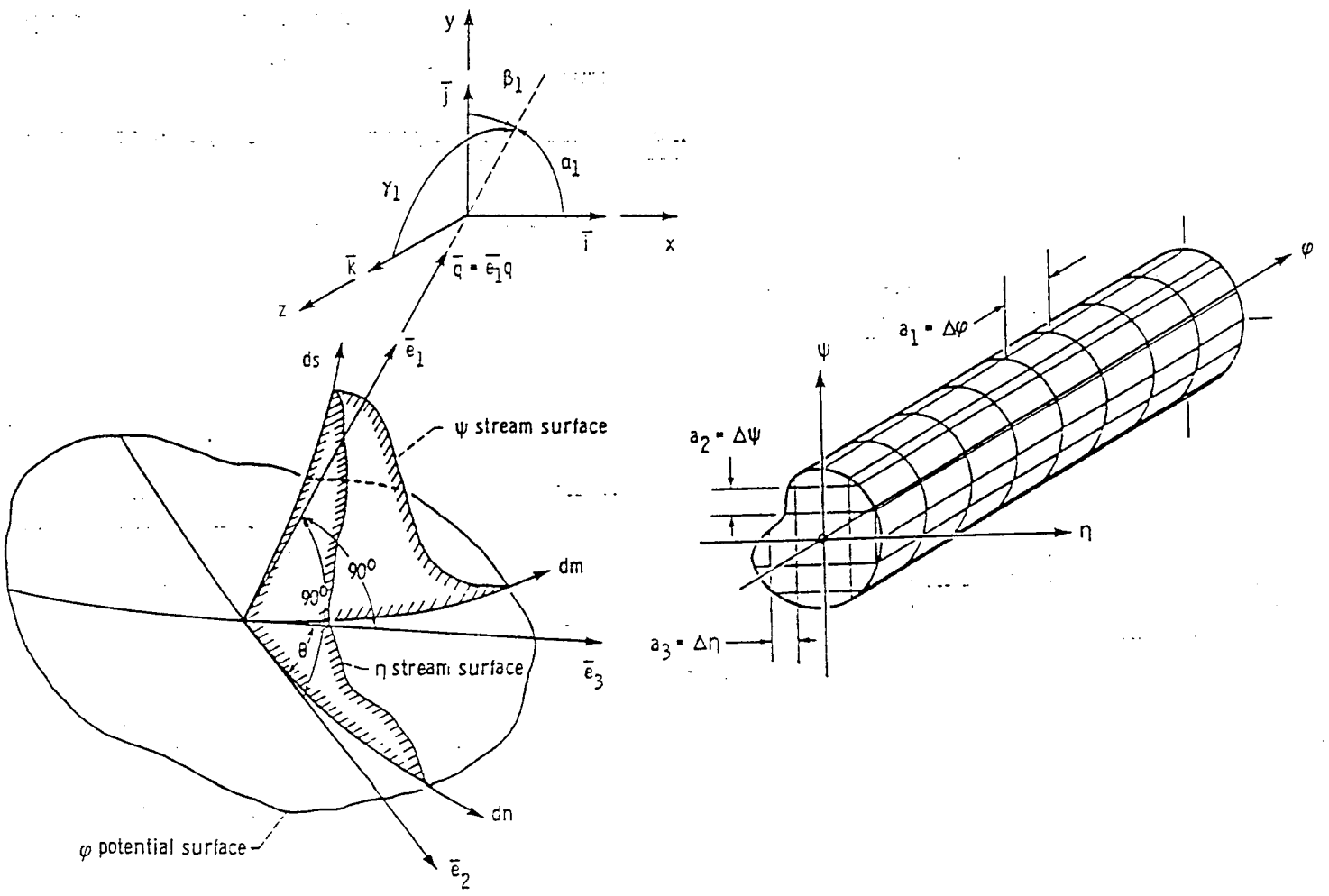

Figure 31(a). -

INPUT FOR NUMERICAL EXAMPLE II

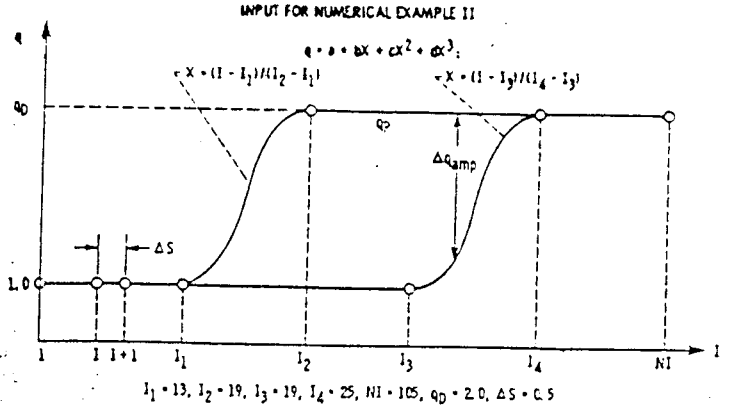

$I_1 = 13$, $I_2 = 19$, $I_3 = 19$, $I_4 = 25$, $NI = 105$, $q_D = 2.0$, $\Delta S = 0.5$

Option ISYM	= 1	Accuracy of finite-difference solution (EPSR)	= 0.000005
Option IVEL	= 1	Overrelaxation factor (DRELAX)	= 1.30
Major iterations (ITER)	= 4	Exit-area error (ERRAR)	= -0.0019
Coefficient to average x, y, z (CAVP)	= 0.2	Running time (370/3033), min	= 103.14
Upstream Mach number (AMU)	= 0.4	DEL-P-01	= 0.3
Ratio of specific heats (GAM)	= 1.4	DEL-P-12	= 0.2
J location of primary streamline (JDO	= 9	DEL-P-23	= 0.3
K location of primary streamline (KDO	= 12	Location of principal streamline (XP)	= 0.9
Number of subdivisions between adjacent input values of I (NSD)	= 3		

Figure 31(b). -

NUMERICAL EXAMPLE II

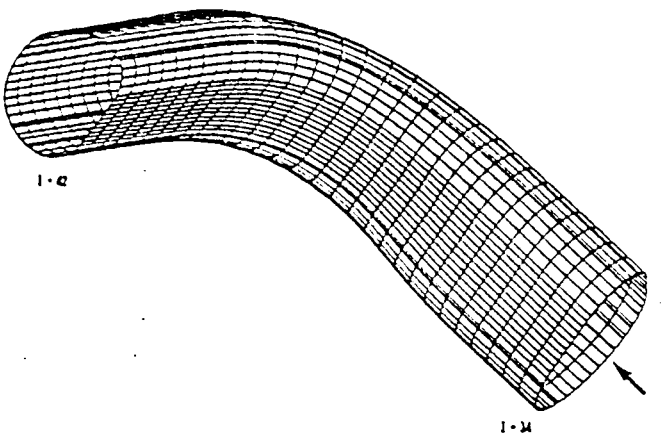

Figure 32(a). -

INPUT FOR NUMERICAL EXAMPLE III

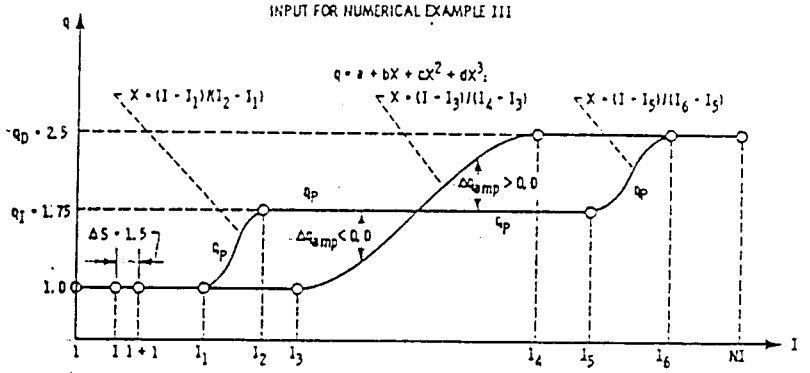

$I_1 = 13$, $I_2 = 19$, $I_3 = 21$, $I_4 = 33$, $I_5 = 41$, $I_6 = 47$, $NI = 59$, $\Delta S = 1.5$

Option ISYM	= 1	;	Accuracy of finite-difference solution (EPSR)	=	0.000005
Option IVEL	= 3	;	Overrelaxation factor (DRELAX)	=	1.30
Major iterations (ITER)	= 10	;	Exit-area error (ERRAR)	=	0.0005
Coefficient to average x, y, z (CAVP)	= 0.2	;	Running time (370/3033), min	=	29.64
Upstream Mach number (AMU)	= 0.3	;	DEL-P-01	=	*
Ratio of specific heats (GAM)	= 1.4	;	DEL-P-12	=	*
J location of primary streamline (JDO	= 4	;	DEL-P-23	=	*
K location of primary streamline (KDO	= 8	;	Location of principal streamline (XP)	=	*
Number of subdivisions between adjacent input values of I (NSD)	= 1	;			

* Not applicable.

Figure 32(b). -

NUMERICAL EXAMPLE III